

X-ray evidence for a mildly relativistic and variable outflow in the luminous Seyfert 1 galaxy Mrk 509

M. Cappi¹, F. Tombesi^{1,2,3,4}, S. Bianchi⁵, M. Dadina¹, M. Giustini^{1,2,6}, G. Malaguti¹, L. Maraschi⁷, G. G. C. Palumbo²,
P. O. Petrucci⁸, G. Ponti⁹, C. Vignali², and T. Yaqoob^{3,4}

¹ INAF-IASF Bologna, via Gobetti 101, 40129 Bologna, Italy
e-mail: cappi@iasfbo.inaf.it

² Dipartimento di Astronomia, Università degli Studi di Bologna, via Ranzani 1, 40127 Bologna, Italy

³ Department of Physics and Astronomy, Johns Hopkins University, 3400, Baltimore, MD 21218, USA

⁴ Laboratory for High Energy Astrophysics, NASA/Goddard Space Flight Center, Greenbelt, MD 20771, USA

⁵ Dipartimento di Fisica, Università degli Studi Roma Tre, via della Vasca Navale 84, 00146, Roma, Italy

⁶ Department of Astronomy & Astrophysics, Pennsylvania State University, University Park, PA 16802, USA

⁷ INAF - Osservatorio Astronomica di Brera, via Brera 28, 20121, Milano, Italy

⁸ Laboratoire d'Astrophysique de Grenoble, Université Joseph-Fourier/CNRS UMR 5571, 38041 Grenoble, France

⁹ APC Université Paris 7 Denis Diderot, 75205 Paris, France

Received 23 March 2009 / Accepted 8 June 2009

ABSTRACT

Context. There is growing evidence for the presence of blueshifted Fe K absorption lines in a number of radio-quiet AGNs and QSOs. These may be fundamental to probe flow dynamics near supermassive black holes.

Aims. Here we aim to verify and better characterise the existence of such Fe K absorption at $\sim 8\text{--}10$ keV in the luminous Seyfert 1 galaxy Mrk 509, one of the most promising target for these studies.

Methods. We present a comprehensive spectral analysis of the six *XMM-Newton* observations of the source (for a total of ~ 200 ks), focusing on a detailed and systematic search for absorption features in the high-energy data.

Results. We detect several absorption features at rest-frame energies $\sim 8\text{--}8.5$ keV and ~ 9.7 keV. The lines are consistent with being produced by H-like iron $K\alpha$ and $K\beta$ shell absorptions associated with an outflow with a mildly relativistic velocity of $\sim 0.14\text{--}0.2$ c. The lines are found to be variable in energy and, marginally, in intensity, implying variations in either the column density, geometry and/or ionization structure of the outflow are common.

Key words. galaxies: active – X-rays: galaxies – accretion, accretion disks – techniques: spectroscopic – line: formation – galaxies: Seyfert

1. Introduction

There is compelling evidence for the presence of blueshifted Fe absorption lines at rest-frame energies of $\sim 7\text{--}10$ keV in the X-ray spectra of several radio-quiet (RQ) AGNs and QSOs. These are commonly interpreted as due to resonant absorption from FeXXV and/or FeXXVI ions associated with a zone of circumnuclear gas with $\log \xi \sim 2\text{--}4$ erg s⁻¹ cm and column density $\sim 10^{22\text{--}24}$ cm⁻² (see Cappi 2006 and references therein), i.e. significantly higher than the absorption layers commonly associated with warm absorbers (Crenshaw et al. 2003; Blustin et al. 2005).

The velocities of these absorbers being often quite large, sometimes reaching mildly relativistic speeds (up to 0.2–0.4 c), suggests that we might be probing the extreme component of a wind/outflow that may well carry large amounts of mass into the interstellar medium (ISM) and/or intergalactic medium (IGM) at a rate comparable to, or even higher than the Eddington accretion rate (King & Pounds 2003; Reeves et al. 2003; Chartas et al. 2003; Pounds & Page 2006).

Most interestingly, variability of the absorption on timescales down to a few ks has been found among some sources (Risaliti et al. 2005; Dasgupta et al. 2005; Braito et al. 2007; Turner et al. 2007; Reeves et al. 2008; Saez et al. 2009;

Giustini et al., in prep.). Variability studies could, in principle, allow us to estimate the location and geometry of the absorber (Nicastro et al. 1999; Krongold et al. 2007; Risaliti et al. 2005; Reeves et al. 2008), thereby placing more stringent limits on the remaining large (order of magnitude) uncertainties in the total mass, energy and momentum that is driven by these outflows (Elvis 2006).

Overall, these studies are fundamental to probe and characterise the most extreme (in terms of velocity, ionization state, mass outflow rate) phases of outflows, thereby helping in quantifying the potential feedback impact of AGNs onto their host galaxies and the IGM.

Mrk 509 ($z = 0.034$) is one of the X-ray brightest (2–10 keV flux of $\sim 2\text{--}5 \times 10^{-11}$ erg cm⁻² s⁻¹) and most luminous ($L_{2\text{--}10 \text{ keV}} \sim 1\text{--}3 \times 10^{44}$ erg/s) Seyfert 1 galaxies known. It is an interesting science case for these studies because a previous study by Dadina et al. (2005), based on *BeppoSAX* multiple observations and on two early *XMM-Newton* observations, found a transient and blueshifted absorption line at a rest-frame energy of ~ 8.2 keV. In addition, a transient, redshifted absorption line at a rest-frame energy of ~ 5.4 keV was found. Motivated by these results, additional monitoring of the source with *XMM-Newton* was then proposed and eventually performed. Here we present

Table 1. Mrk 509 XMM-Newton observation log.

N°	Obs. ID	Date	Expo	Counts
			(ks)	(2–10 keV)
				($\times 10^4$)
1	0130720101	2000 Oct. 25–25	20.7	7
2	0130720201	2001 Apr. 20–20	23.1	10
3	0306090101	2005 Oct. 16–16	2.7	1.1
4	0306090201	2005 Oct. 18–19	59.8	25
5	0306090301	2005 Oct. 20–20	32.4	14
6	0306090401	2006 Apr. 25–26	48.6	23

Number, Observation ID, Observation date, net EPIC pn exposure time, and total 2–10 keV counts for the six *XMM-Newton* observations of Mrk 509.

the results on the systematic search for and characterization of Fe *absorption* lines at high energies obtained from a comprehensive analysis of the full set of six *XMM-Newton* observations¹.

2. Data analysis and results

Mrk 509 was observed by the *XMM-Newton* EPIC instruments on six separate occasions, for a total good exposure time of ~ 280 ks (see Table 1). The observations were performed once in October 2000, once in April 2001, three times in October 2005, and once in April 2006. The only contiguous observations were those performed in 2005. The data were reduced using the standard software SAS v. 8 (de la Calle & Loiseau 2008) and the analysis was carried out using the HEASoft v. 6.5 package². After filtering for times of high background rate, the useful exposure times, corrected for the live time fraction (up to 0.7 for the pn in small window mode), were between 2.7 and 60 ks per observation (see Table 1). The EPIC pn and MOS cameras were operated in the “small window” mode with the thin filter applied for all observations. We checked that pile-up was not significant in the pn data at this level of source flux, even when considering both single and double events. The pile-up fraction for the MOS data was $\lesssim 15\%$ for all observations. In this case, this will not affect the results on the narrow absorption lines presented in this work. Source counts were extracted from a circular region of 40 arcsec radius, while the background counts were extracted from a nearby source-free area of the detector of the same size. Given the significantly lower effective area of the MOS detector between 6–10 keV, and for clarity and simplicity, we only report here the results obtained from the pn data and show the MOS data for consistency checks only. We decided also not to report the observation n. 3 because its very short exposure (~ 2.7 ks; see Table 1) hampered any significant analysis.

2.1. Light-curves

Analysis of the soft and hard X-ray light curves from the six observations indicates only moderate (~ 20 – 30%) flux and spectral variability on both short ($< \text{few tens ks}$) and long ($\sim \text{years}$) time-scales (see lightcurve in Fig. 1 of Ponti et al. 2009). A more detailed time-resolved spectral analysis focused on the low-energy warm absorber as measured by the RGS is deferred to a specific paper (Detmers et al., in preparation).

¹ Results on the Fe *emission* line properties, for the same dataset, were presented in Ponti et al. 2009.

² <http://heasarc.gsfc.nasa.gov/docs/software/lheasoft/>

Table 2. 3.5–10.5 keV continuum and Fe emission line parameters.

N°	Γ	Energy ¹	EW^2	Flux ³	χ^2/ν	$\Delta\chi^2$
		(keV)	(eV)			
1	1.55 ± 0.03	6.37 ± 0.03	82 ± 40	3.0	924/850	61
2	1.60 ± 0.03	6.41 ± 0.04	60 ± 30	3.8	992/991	42
4	1.70 ± 0.02	6.41 ± 0.02	65 ± 20	3.5	1151/1194	130
5	1.72 ± 0.03	6.41 ± 0.03	62 ± 28	3.6	990/1012	67
6	1.69 ± 0.02	6.43 ± 0.03	58 ± 20	4.2	1175/1189	101

¹ Emission line rest-frame energy centroid, in units of keV; ² Emission line rest-frame equivalent width, in units of eV. The width of the line was fixed to $\sigma = 0.1$ keV (see text for details); ³ 2–10 keV flux in units of 10^{-11} erg s^{-1} cm^{-2} .

2.2. X-ray continuum and Fe emission lines

Given the weakly varying continuum, we extracted the mean pn spectra for each of the six observations, grouping the data to a minimum of 25 counts per channel to apply the χ^2 minimization statistics. Only the data in the 3.5–10.5 keV interval were considered, and the signal-to-noise ratios, even at 10 keV, were always greater than 12 (pn) and 6 (MOS). The spectra were first fitted with a single power-law model plus a column density with a value fixed at the Galactic one ($N_{\text{Hgal}} \approx 4 \times 10^{20}$ cm^{-2} , Dickey & Lockman 1990). We checked that the addition of a further neutral absorption component intrinsic to the source was not required by the data. We obtained good fits of the continuum with a typical power-law photon index of $\Gamma \approx 1.55$ – 1.72 , but residuals of the data (Fig. 1, top panel) clearly showed the presence of a neutral Fe $K\alpha$ emission line at the rest frame energy of ~ 6.4 keV. We therefore added a Gaussian emission line to the model. The line was slightly resolved (see also Ponti et al. 2009), and we fixed the width σ to its best-fit value of ~ 100 eV. Best-fit values with this simple model are reported in Table 2, with errors quoted at the 90% confidence level. The fit improvement was of $\Delta\chi^2 \geq 42$ and the equivalent width of the emission line of the order of ~ 60 – 80 eV for all the observations.

In a few observations (namely observations 4, 5 and 6) we found additional weak, but significant, residuals blueward of the 6.4 keV due to presumably Fe $K\beta$ emission plus higher ionization iron emission components. Indeed, using this same dataset, together with a ~ 100 ks Suzaku observation that partially (for ~ 25 ks) overlapped the observation n. 6, Ponti et al. (2009) have shown in a companion paper that this emission could be well reproduced by a broad line from an accretion disc, while it cannot be easily described by scattering or emission from photo-ionized gas at rest. We did not investigate nor consider further these emission structures here, since the primary aim of the present work is to perform a detailed search for absorption lines at energies above ~ 7 keV. We checked nevertheless that different parameterizations and/or modelling of the complex Fe emission line structure, including the above weak ionized components, do not affect the results and conclusions presented here.

2.3. Fe absorption lines

Dadina et al. (2005) reported the detection of both red- and blue-shifted absorption lines due to highly ionized Fe in the *BeppoSAX* and *XMM-Newton* (non-simultaneous) spectra of Mrk 509. These lines were found at rest-frame energies of ~ 5.5 keV and ~ 8.2 keV, respectively. The first was seen in two *BeppoSAX* observations, the latter was seen by both satellites. Motivated by these results, we performed a systematic and blind

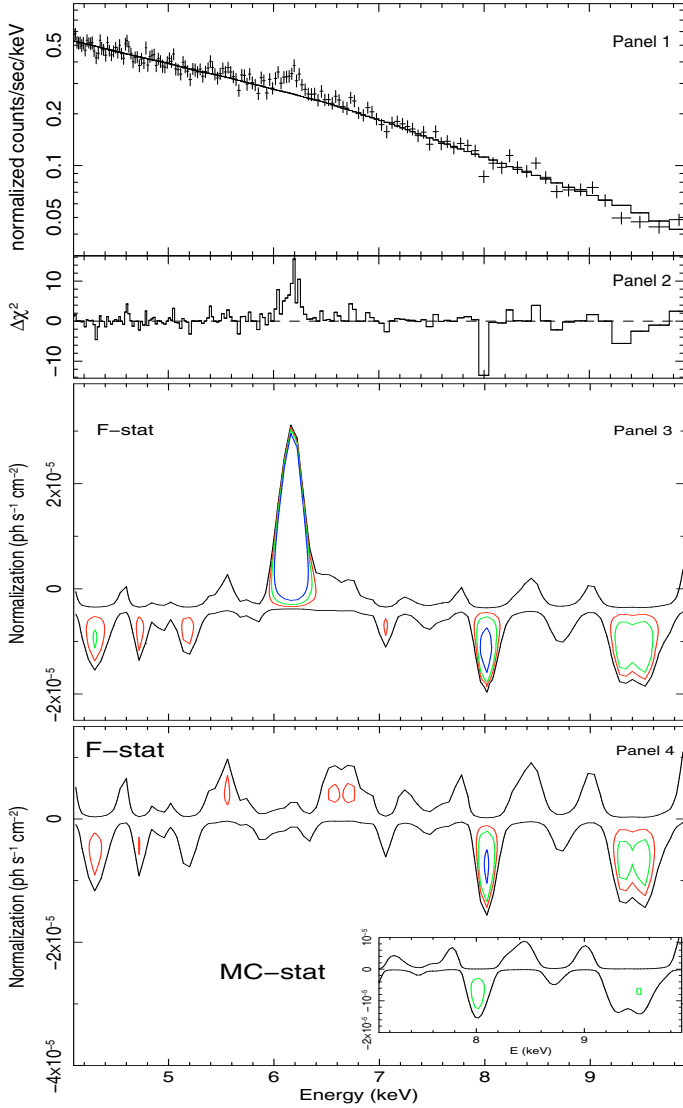


Fig. 1. *Panel 1:* EPIC pn spectrum of Mrk 509 (obs. 1) fitted in the 3.5–10.5 keV band, with data rebinned with $S/N > 12$, fitted with a single power-law model; *Panel 2:* $\Delta\chi^2$ residuals; *Panel 3:* F-statistics confidence contours (68% (red), 90% (green) and 99% (blue) levels) with a single power-law model with Galactic absorption; *Panel 4:* F-statistics confidence contours (68%, 90% and 99% levels) after the inclusion of a Gaussian emission line in the model; and *Panel 4, inset:* Confidence contours between 7–10 keV calculated using a Monte Carlo simulation (see text for details). Contours (in black) calculated with $\Delta\chi^2 = 0.5$ are reported to indicate the continuum level.

search for absorption structures in the ~ 4 –10 keV band for the whole *XMM-Newton* dataset available to date.

We first fitted the 3.5–10.5 keV data with a simple power-law model and searched for deviations in the $\Delta\chi^2$, as shown in the first and second panels of Fig. 1 for observation 1. We then implemented a more systematic method to search for features in the spectrum, similar to the one introduced by Miniutti & Fabian (2006) and Miniutti et al. (2007). We fitted the 3.5–10.5 keV data with the baseline power-law only (panel 3) or with the power-law plus Gaussian emission line model (panel 4) obtained in Sect. 2.2, stored the resulting χ^2 value, and then froze the baseline model parameters to their best-fit values. We then added a narrow (unresolved, $\sigma = 0.01$ keV) Gaussian line to the model, and then searched for the presence of both emission and absorption features by making a series of fits stepping the new Gaussian

line energy in either the 4–10 keV or 7–10 keV intervals and its normalization between -4×10^{-5} and $+4 \times 10^{-5}$ $\text{ph s}^{-1} \text{cm}^{-2}$, each time storing the new χ^2_i value. We then derived a grid of χ^2 values and made a plot of the contours with same $\Delta\chi^2$ level with respect to the baseline model fit. Negative $\Delta\chi^2$ values calculated in this way indicate that a better fit is reached with the inclusion of the line and, like in the standard *steppar* type of contours in XSPEC, the $\Delta\chi^2$ values can be translated into a statistical confidence level for the addition of 2 more parameters, as these do not depend on the sign but only on the absolute value of $\Delta\chi^2$. We then plot the standard values of $\Delta\chi^2 = -2.3$, -4.61 and -9.21 relative to confidence levels of 68%, 90% and 99%, respectively. The major difference between these contours and the standard ones obtained with the *steppar* command in XSPEC is that the contours are here “inverted” in the sense that inner contours have a higher significance than outer ones. These contours are shown in panel 3 and 4 of Fig. 1, for observation 1, as well as in Figs. 2 and 3, for all the observations.

The probability levels shown in Fig. 1 are derived from F-test statistics only, and do not take into account the number of trials used by our blind line search technique approach (e.g. Protassov et al. 2002). This might result in an overestimation of the statistical significance associated with each line feature. For this reason, contours derived with a method based on Monte Carlo simulations are shown for observation 1, in the inset of Panel 4 of Fig. 1. We address issues and results from this method further in Sect. 2.4 below.

As for the redshifted absorption structures, we noted the presence in the data of weak deviations between 4 and 6 keV (see the residuals redward of the FeK emission line in Fig. 2). After inclusion of the neutral FeK emission line in the fit, we found that none of these absorption features is, however, statistically significant, with upper-limits for an absorption line in that energy range of $EW \gtrsim -15$ eV (90% confidence). We did not confirm therefore the two positive BeppoSAX detections of the redshifted absorption line but our data are still consistent with a scenario where the absorber is transient and/or patchy in nature, as proposed in Dadina et al. (2005).

As for the blueshifted absorption structures, we find instead several in the data. Not only is the previous *XMM-Newton* detection during observation 1 by Dadina et al. (2005) confirmed, but the line is detected at a high significance level (see Table 3, and Figs. 2 and 3) also during observations 4 and 6 (at $E \sim 8.2$, 8.0 and 8.4 keV, respectively). In addition, there is evidence during both observations 1 and 6 that an additional absorption line, possibly broader or maybe due to a blend of lines, is present at even higher energies, at $E \sim 9.4$ keV (observed frame), i.e. ~ 9.7 keV (rest-frame). Confidence contours for these absorption lines are shown in Figs. 2 and 3. We report in Table 3 the best-fit parameters for these lines, as well as the significance of their detections, calculated with the F-statistics (Col. 5) and the Monte Carlo simulations (Col. 6).

Remarkably, the two sets of two lines are consistent with the theoretical energy peaks of FeXXVI $K\alpha$ (6.966 keV) and $K\beta$ (8.268 keV), if blueshifted with respect to the systemic velocity by $v \sim 0.17c$ (obs. 1) and $v \sim 0.2c$ (obs. 6), respectively. The line at ~ 8 keV during obs. 4 is consistent with Fe XXVI $K\alpha$ at $v \sim 0.14c$. If the lines were associated, instead, with FeXXV $K\alpha$ (6.697 keV) and $K\beta$ (7.880 keV), the required velocity shifts would be consequently larger (i.e. $v = 0.21$, 0.18 and 0.23c for obs. 1, 4 and 6, respectively).

We also checked the MOS results for consistency with the pn instrument. Remarkably, despite the considerably lower statistics for the MOS (due to the much lower effective area at

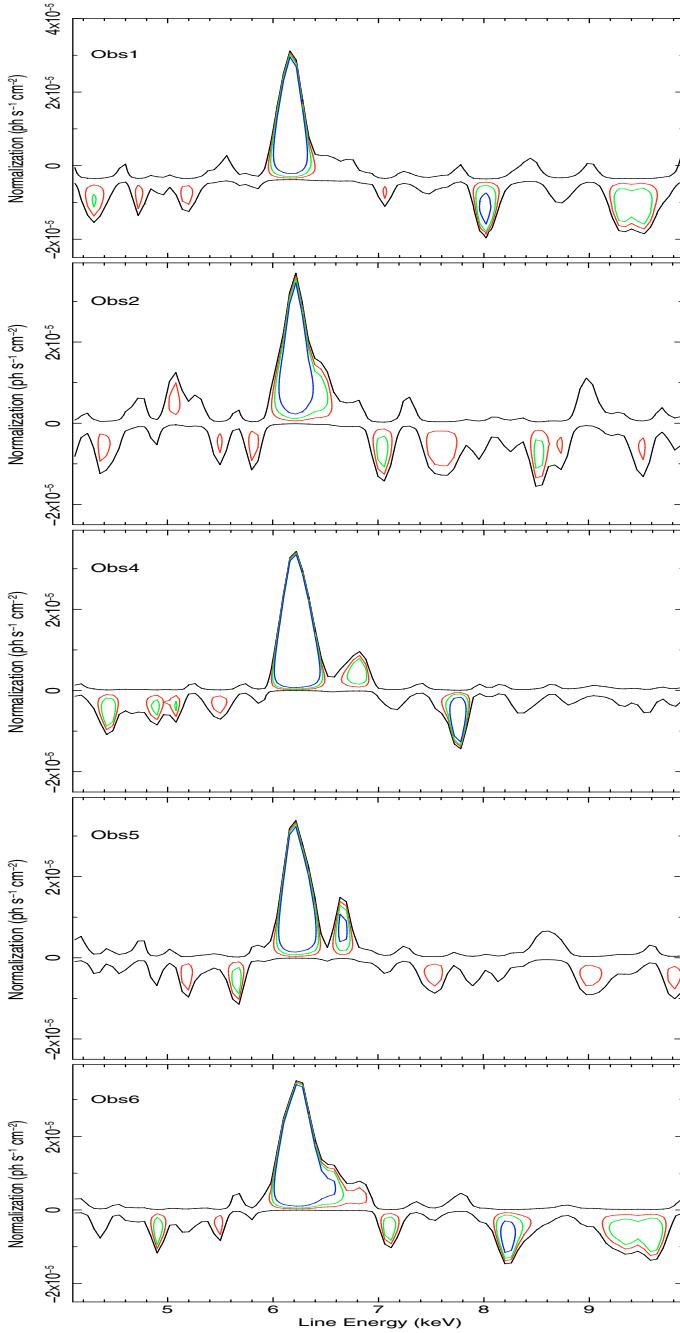


Fig. 2. 4–10 keV confidence contours for $\Delta\chi^2 = -2.3$, -4.61 and -9.21 (i.e., 68%, 90% and 99% levels) calculated for both positive and negative residuals for a narrow Gaussian line in the data over the 4–10 keV energy range (see text for details). The contours at $\Delta\chi^2 = +0.5$ are also reported.

$E > 7$ keV), we found evidence, albeit with lower significance, of absorption features in all three observations 1, 4 and 6 and with energies and intensities consistent with the pn. In particular, we found statistical improvements by $\Delta\chi^2 = 13$, 5 and 3, for the addition of a line at $E \sim 8.2$, 8.0 and 8.4 keV, with $EW \simeq -67 \pm 30$ eV, -24 ± 23 eV, and -17 ± 16 eV (at a 90% confidence for one additional d.o.f.), respectively. These results suggest that these lines are not statistical artifacts (but see also Sect. 2.4).

The pn background spectrum is known to have two instrumental emission features, one at an observed energy of ~ 7.5 keV

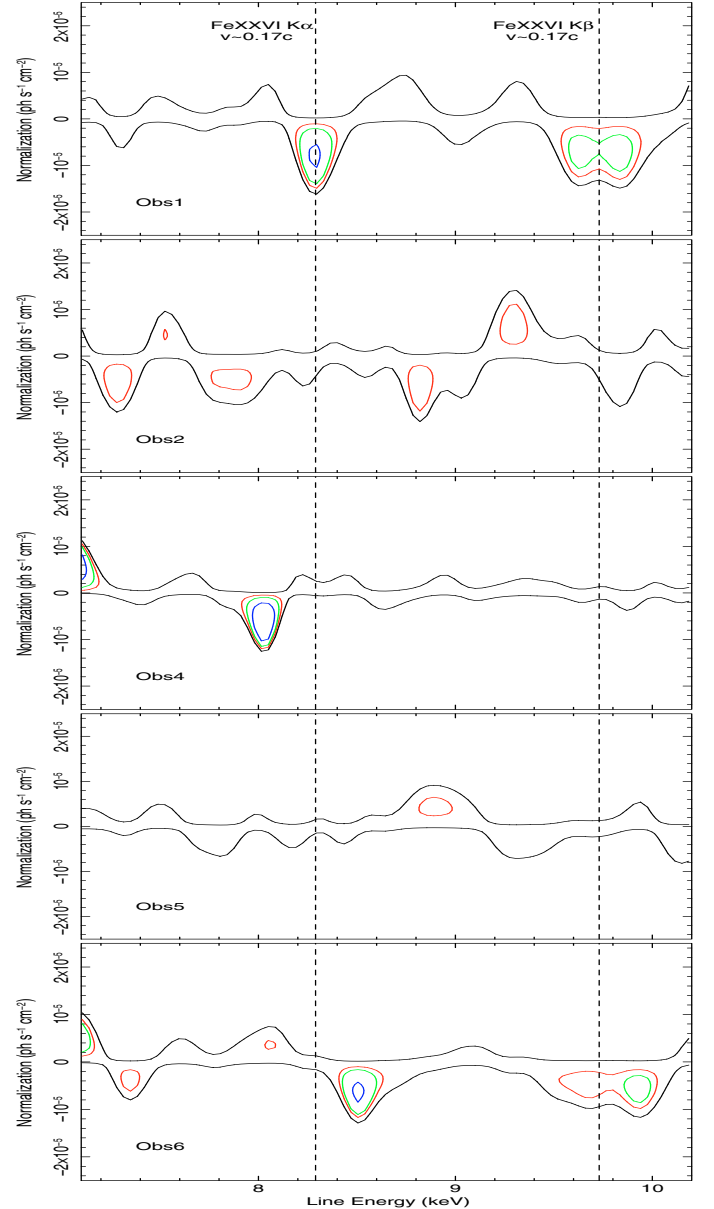


Fig. 3. Zoomed, rest-frame 7–10 keV confidence contours for $\Delta\chi^2 = -2.3$, -4.61 and -9.21 (i.e., 68%, 90% and 99% levels, colors are as those in Fig. 1) calculated for both positive and negative residuals for a narrow Gaussian line in the data between 7–10 keV (see text for details). The contours at $\Delta\chi^2 = +0.5$ are also reported.

due to an Ni K α emission line and one at ~ 8 keV due to a Cu K α emission line (Katayama et al. 2004; Freyberg et al. 2004). These may have a strong impact on the source high-energy spectrum. We checked, however, that this is not the case for Mrk 509. The source is so bright ($F(2-10 \text{ keV}) > 2 \times 10^{-11} \text{ erg cm}^{-2} \text{ s}^{-1}$) that the background level was always negligibly small, even in the FeK bandpass and for both pn and MOS (see Fig. 4), thereby excluding a possible artifact due to the instrumental background.

During observations 2, 4 (for the ~ 9.7 keV line) and 5, where the features were not detected, we obtained upper limits on the absorption lines at energies of $E \simeq 8.3$ and 9.7 keV, with $EW \gtrsim -15$ and $\gtrsim -30$ eV, respectively (see Table 3).

Finally, there are indications that the lines do vary among the observations (see Fig. 3, where contours are plotted at rest-frame energies), clearly in blueshift/energy (being 0.17c, 0.14c and 0.20c during obs. 1, 4 and 6 respectively) and possibly in

Table 3. Mrk 509 absorption line parameters (rest-frame energies).

N obs.	E^a (keV)	EW^a (eV)	$\Delta\chi^2$	F-test	MC ^b	Id (FeXXVI)	v/c
1	8.29 ± 0.05	-32 ± 20	9.6	$\sim 99\%$	95%	K α	0.172 ± 0.005
	9.74 ± 0.09	-59^{+18}_{-22}	8	$\sim 98.5\%$	87.5%	K β	0.162 ± 0.009
2	$\equiv 8.29^c$	$\gtrsim -23$		
	$\equiv 9.74^c$	$\gtrsim -32$		
4	8.03 ± 0.03	-20 ± 10	16.5	$\gtrsim 99.9\%$	99.8%	K α	0.141 ± 0.003
	$\equiv 9.74^c$	$\gtrsim -17$		
5	$\equiv 8.29^c$	$\gtrsim -14$		
	$\equiv 9.74^c$	$\gtrsim -17$		
6	8.50 ± 0.05	-20 ± 12	10.2	$\sim 99.5\%$	95.5%	K α	0.196 ± 0.005
	$9.8^{+0.1}_{-0.2}$	-34^{+26}_{-29}	7	$\sim 98\%$	78%	K β	$0.17^{+0.02}_{-0.01}$

^a Rest-frame energy. Errors are quoted at the 90% and 68% confidence for the first and second lines, respectively. ^b Significance calculated through Monte Carlo simulations. ^c Values frozen at the best-fit values obtained during obs. 1.

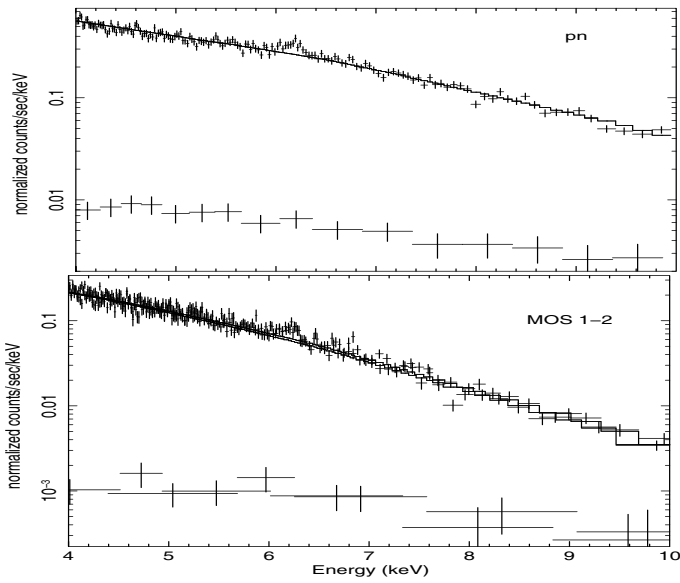


Fig. 4. pn source and background during obs. 1 (Top), rebinned with $S/N > 12$; MOS source and background during obs. 1 (Bottom), rebinned with $S/N > 6$ and 3, respectively. The spectra show that the source is over an order of magnitude higher in counts $s^{-1} \text{ keV}^{-1}$ compared to the backgrounds in the FeK bandpass, in both pn and MOS.

intensity, since they were not detected during observations 2 and 5. In particular, albeit marginal, the intensity variations are found on a time-scale as short as ~ 100 ks, i.e. the time between obs. 4 and 5, but one should recall the intrinsic difficulty of placing stringent upper limits on the EW of lines for which the velocity is unknown a-priori. The line velocity variations are instead unambiguous (see Fig. 3), on a time-scale of ~ 6 months, i.e. the time between obs. 4 and obs. 6. Given the mass of the black hole in Mrk 509 of $M_{\text{bh}} \sim 1.4 \pm 0.1 \times 10^8 M_{\odot}$ (Peterson et al. 2004), such variability time-scales suggest the presence of important radial or transverse motion quite close to the central supermassive black hole, as discussed below.

2.4. On the statistical significance of the absorption lines

The F-test detection probabilities derived here (see Table 3) from our line blind search can be overestimates of their real values (e.g. Protassov et al. 2002). We therefore applied a more rigorous method that uses extensive Monte Carlo simulations (see e.g. Porquet et al. 2004; Miniutti & Fabian 2006;

Markowitz et al. 2006) in order to assess the detection probabilities from our line blind search. For all three cases in which one or two lines have been detected (i.e. observations 1, 4 and 6), we considered the absorbed power law plus narrow Gaussian emission line as the null-hypothesis model.

We simulated a null-hypothesis model spectrum with the same exposure as the real data and subtracted the appropriate background. This spectrum was fitted again with the null-hypothesis model in the 3.5–10.5 keV band and the new parameters were recorded. Then, we generated a new simulated spectrum with this refined null-hypothesis model in order to account for the uncertainties in the model itself. Therefore, we made a fit of the null-hypothesis model to this new simulated spectrum, considering only the 3.5–10.5 keV band and recorded the χ^2 value. We then added a narrow Gaussian line ($\sigma = 0.01$ keV) to the model, with its normalization free to be positive or negative and stepped the centroid energy between 7 and 10 keV at intervals of 100 eV. Each time we made a new fit and recorded the maximum of these simulated $\Delta\chi^2$. Then, we repeated the above procedure $S = 10^4$ times in order to generate a distribution of 10^4 simulated $\Delta\chi^2$ values. If N simulated $\Delta\chi^2$ values were greater than or equal to the real one, then the detection confidence level corresponds to $1 - N/S$.

The new values of line detection confidence levels based on the above Monte Carlo simulations are reported in Table 3, in comparison to the F-test probabilities. We also estimated the combined Poissonian probability of detecting by chance the 3 absorption lines (at $E \sim 8$ –8.5 keV) in 5 observations, and this turned out to be ≤ 0.001 (i.e. a probability $\geq 99.9\%$ that these lines are not artifacts). Considering also the two lines at $E \sim 9.7$ –9.8 keV, and that they turn out to be at the expected energies for K β transitions (i.e. the F-statistics alone should work properly for these), this would lower the combined probability even further. For example, a fit with the two lines (FeXXVI K α and K β) with their energies fixed at their theoretically expected values, and same blueshifted velocity, yielded a $\Delta\chi^2$ improvement of 19 and 13, for 3 interesting parameters, corresponding to a probability of $>99.9\%$ and 99.5% during observations 1 and 6, respectively.

3. Discussion and conclusions

The main results of our spectral analysis are the following:

- We detected several absorption features in the energy range ~ 8 –10 keV in three (out of six) *XMM-Newton* observations

of the bright and luminous Seyfert 1 galaxy Mrk 509. The equivalent widths of the lines are between -20 and -60 eV.

- The most likely identification for these features being FeXXVI $K\alpha$ and $K\beta$, they imply (mildly) relativistic blueshifts in the range ~ 0.14 – $0.2c$, and low $K\alpha/K\beta$ ratios, of the order of unity.
- There is evidence for line velocity variations, as well as for the appearance and disappearance of the lines, on time-scales as short as ~ 100 ks.

The above results are reminiscent of the Seyfert 1.5 NGC 1365 (Risaliti et al. 2005), in particular for i) the identification of the absorption lines with FeXXVI $K\alpha$ and $K\beta$ lines; ii) the small $K\alpha/K\beta$ ratios; and iii) the velocity variations detected on similarly short time-scales for a comparable black hole mass. Differences are that here we only detect one ionization state for iron (instead of two, FeXXV and FeXXVI, for NGC 1365), and the line velocities are about ten times larger than in NGC 1365. As shown below, this could be due to an intrinsically more extreme outflow in Mrk 509 with respect to NGC 1365, in terms of either velocity or ionization state, or both. Alternatively, the structure and velocity field of radiatively-driven winds being a function of the polar angle (e.g. Proga & Kallman 2004), a different viewing angle as expected for their type 1 (for Mrk509) and type 2 (NGC 1365) classification would naturally imply different average velocities along the line of sight.

Outflowing material is expected to imprint a characteristic P-Cygni profile on the data, where the detailed absorption and re-emission line profile depends strongly on the flow/wind geometry and density. Theoretical predictions based on Monte Carlo calculations have been presented in, e.g., Schurch & Done (2007) and Sim et al. (2008), with some recent attempts to fit the best available observational data (Sim et al. 2008; Pounds & Reeves 2008). Rather than attempting here such a full treatment and modelling of the absorber with data of admittedly too low statistical significance for such a purpose, we discuss the above results in the light of simpler and more qualitative arguments.

Following Risaliti et al. (2005) and from the curves of growth presented in Bianchi et al. (2005), an equivalent width of the $K\alpha$ lines $EW \sim 20$ – 30 eV can be obtained with $N_{\text{H}} \gtrsim 5 \times 10^{23} \text{ cm}^{-2}$ and $\log \xi \gtrsim 4 \text{ erg cm s}^{-1}$, with turbulent velocity set to zero. With larger values of turbulence, i.e. velocities between 100 and 1000 km s^{-1} , the column density does not need to be as large, with values of $N_{\text{H}} \sim 5$ – $10 \times 10^{22} \text{ cm}^{-2}$. These values would also be consistent with the low $K\alpha/K\beta$ ratios, which indicate that saturation effects are significant (see Fig. 4 in Risaliti et al. 2005). Given the low statistics available, velocity widths as large as a few thousand km/s, i.e. consistent with the above estimates, cannot be excluded here. Such high values of turbulence would also be reasonable for bulk motion in an outflow with such large velocities.

These rough estimates were then confirmed through a more detailed, but still approximate, fitting of the FeK absorption lines with two different phenomenological models: *zxcipf*, a partial covering of photo-ionised absorbing material that is incorporated into the XSPEC package (Reeves et al. 2008), and XSTAR tables calculated using an input SED with a power-law photon index of $\Gamma = 2$ and a turbulent velocity of 1000 km s^{-1} . We obtained good and consistent fits to the data. For all three observations (obs. 1, 4 and 6), the best-fit parameter values were $\log \xi \sim 5 \pm 0.4 \text{ erg cm s}^{-1}$, $N_{\text{H}} \sim 2$ – $4 \times 10^{23} \text{ cm}^{-2}$ and a blueshift of $v \sim 0.14$ – $0.2c$. Best-fit models obtained with the XSTAR photoionization model are shown in Fig. 5. In these models, the lines are produced by only FeXXVI ($K\alpha$ and $K\beta$) and, despite the

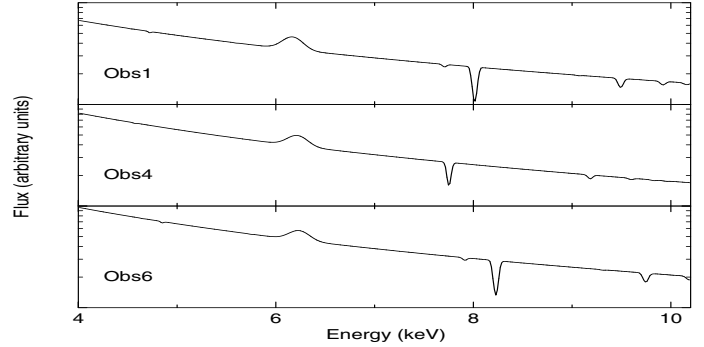


Fig. 5. Best-fit photoionized models for observations n.1 (top), 4 (middle) and 6 (bottom). See text for details.

large columns, no other signature is expected at lower energies because of the extremely high ionization.

Another possible solution, albeit slightly statistically worse, could also fit the EPIC data with less extreme values of $N_{\text{H}} \sim 10^{22-23} \text{ cm}^{-2}$ and $\log \xi \sim 3 \text{ erg s}^{-1} \text{ cm}$. In this case, the absorption lines are identified with mainly FeXXV. This solution does, however, require even larger velocities, up to 0.18 – $0.23c$. Moreover this solution appears to be slightly fine-tuned because a slightly lower value of ξ would imply a significant low-energy curvature and a higher value of ξ would give rise to lines also from FeXXVI. We checked but did not find any evidence in the RGS data of OVIII absorption lines at the above-mentioned velocities, the data yielding quite stringent limits of $EW \lesssim 0.2$ – 0.4 eV. Altogether, this solution appears to be less likely than the one based on FeXXVI “only” and was thus not considered any further here.

The high ionization parameter, together with the variations seen in the absorption lines, can be used to infer limits on the distance and size of the absorber. Assuming that the ionization state is due to illumination from the central X-ray and UV source, rather than heated/illuminated locally, we can use $\xi = L_{\text{ion}}/(nr^2)$, where n is the number density, and L_{ion} the source continuum luminosity (integrated between 1 and 1000 Rydberg) to estimate the maximum distance r of the absorber from the illuminating source. The observed line-of-sight absorbing column N_{H} is a function of the density n of the material at an ionisation parameter ξ and the shell thickness Δr : $N_{\text{H}} = n\Delta r$. Making the reasonable assumption (given the $r^{-\alpha}$ dependencies of winds/outflows) that the thickness Δr is less than its distance from the source r , and combining the expression for the ionisation parameter, we obtain the limit $r < L_{\text{ion}}/(\xi N_{\text{H}})$. Using $L_{\text{ion}} = 2 \times 10^{44} \text{ erg/s}$, $N_{\text{H}} = 10^{23} \text{ cm}^{-2}$ and $\log \xi \sim 5 \text{ erg cm s}^{-1}$, we obtain $r \leq 2 \times 10^{16} \text{ cm}$. Assuming the black hole mass of $M_{\text{bh}} = 1.4 \times 10^8 M_{\odot}$ (Peterson et al. 2004) for Mrk 509, this corresponds to a location for the absorber within a distance < 500 Schwarzschild radii (r_s) from the black hole.

Interestingly, we note that the variability of the absorption lines is indicative of a compact absorber and rules out a local origin, from either the Galaxy or the Local Group, for the absorber (McKernan et al. 2004, 2005). In fact, the absorber appears to be even more compact than the broad line region, which has an estimated size of the order of ~ 80 light-days (Kaspi et al. 2005). Analogous short term variability of iron absorption line velocity and intensity was recently found for the BAL QSO APM 08279+5255 (Saez et al. 2009), suggesting that rapid changes in the geometry of the outflow and/or of physical parameters of the absorber are a fundamental characteristic of the X-ray component of AGN winds.

A rough estimate of the escape velocity along the distance of a Keplerian disk is given by the equation $v^2 = 2GM/r$, which can be written as $v = (r_s/r)^{1/2}c$. The observed blueshift velocity of the absorber $v \sim 0.14\text{--}0.2c$ is therefore much larger than the escape velocity at $\sim 500 r_s$, of the order of $\sim 0.05c$, as well as the escape velocity at $100 r_s$, that is $\sim 0.1c$. Assuming a constant velocity for the outflow and the conservation of the total mass, we can thus estimate the mass loss rate \dot{M}_{out} associated with this outflow as $\dot{M}_{\text{out}} \sim \Omega n r^2 v m_p$, where v is the outflow velocity, n is the ion number density of the absorber, m_p is the proton mass and Ω is the covering fraction of the outflow. Following Blustin et al. (2005), this translates to $\dot{M}_{\text{out}} \sim 1.23 m_p \frac{L_{\text{ion}}}{\xi} \Omega v$, i.e. for Mrk509, to $\dot{M}_{\text{out}} \lesssim 2.4 \times (\Omega/4\pi) v_{0.1} M_{\odot} \text{ yr}^{-1}$, with $v_{0.1}$ the flow velocity in units of $0.1c$. This corresponds then to a kinetic power of $\frac{1}{2} \dot{M}_{\text{out}} v^2 \lesssim 6.7 \times 10^{44} (\Omega/4\pi) v_{0.1}^3 \text{ erg s}^{-1}$ that could be injected into the ISM.

Following McKernan et al. (2007), we can derive a simple relation for the ratio between the mass outflow rate and the rate of the accretion flow, i.e. $\dot{M}_{\text{out}}/\dot{M}_{\text{acc}} \sim 6000 (\Omega/4\pi)(v_{0.1}/\xi_{100})\eta_{0.1}$, where Ω is the absorber covering fraction, ξ_{100} is the ionization parameter in units of $100 \text{ erg cm s}^{-1}$ and $\eta = \eta_{0.1} \times 0.1$ is the accretion efficiency of the black hole. For Mrk 509, this relation yields $\dot{M}_{\text{out}}/\dot{M}_{\text{acc}} \sim 10 (\Omega/4\pi)$, implying either a low covering fraction and/or an intermittent outflow to permit the growth of the black hole. Viceversa, even a moderately large covering factor for the outflow would imply significant and energetically relevant mass losses into the ISM.

The high velocity, high ionization and variability properties of this absorber suggest that it may be associated with an outflow launched by an accretion disk at relatively small radii of less than a few hundred Schwarzschild radii. This adds to the well known evidence from the soft X-rays of a multi-phase warm absorber in Mrk 509 with $\log \xi \sim 0.9\text{--}3.26$ and $N_{\text{H}} \sim 0.8\text{--}5.8 \times 10^{21} \text{ cm}^{-2}$ (Smith et al. 2007), and to the “intermediate” ($\log \xi \sim 5.4$, $N_{\text{H}} \sim 5.8 \times 10^{22} \text{ cm}^{-2}$ and $v \sim 0.05c$) absorption component found by Ponti et al. (2009) based on continuum variability arguments. Overall, Mrk 509 shows compelling evidence for a stratified absorber, as those predicted by hydrodynamical simulations of radiatively and/or magnetically driven outflows (Proga 2003; Proga & Kallman 2004; King & Pounds 2003; Murray et al. 1995), but with ionizations and velocities up to extreme and challenging values. The extreme ionization parameter raises the question as to how much more fully ionised matter is included, but undetected yet, in the outflow, with its implications for the outflow mass-loss rates and energetics.

Finally, the frequency in AGNs of such extreme outflows is to date unclear. Proper statistical studies on larger, complete samples are being performed (Tombesi et al., in preparation). They are needed to secure the statistical significance of these features, and to assess their frequency and typical characterisation in terms of density, velocities, ionization states and covering factor. Unfortunately, currently available data do suffer an “observational bias” against the detection of the highest-velocity blueshifted features in that orbiting X-ray telescopes are of limited spectral and sensitivity capabilities at $E > 7 \text{ keV}$. Future missions such as *IXO* will likely allow an exciting step forward

in studying mildly relativistic outflows in AGNs, as demonstrated by the first attempted simulations (Cappi et al. 2008; Tombesi et al. 2008).

Acknowledgements. This paper is based on observations obtained with the *XMM-Newton* satellite, an ESA funded mission with contributions by ESA Member States and USA. We would like to thank the referee K. Pounds for his constructive suggestions. We thank A. De Rosa for useful discussions. M.C., S.B., M.D. and G.P. acknowledge financial support from ASI under contracts ASI/INAF I/023/05/0 and I/088/06/0. GP acknowledges ANR for support under grant number ANR-06-JCJC-0047.

References

- Bianchi, S., Matt, G., Nicastro, F., Porquet, D., & Dubau, J. 2005, *MNRAS*, 357, 599
- Blustin, A. J., Page, M. J., Fuerst, S. V., Branduardi-Raymont, G., & Ashton, C. E. 2005, *A&A*, 431, 111
- Braitto, V., Reeves, J. N., Dewangan, G. C., et al. 2007, *ApJ*, 670, 978
- Cappi, M. 2006, *Astron. Nachr.*, 327, 1012
- Cappi, M., Tombesi, F., & Giustini, M. 2008, *Mem. Soc. Astron. Ital.*, 79, 123
- Chartas, G., Brandt, W. N., & Gallagher, S. C. 2003, *ApJ*, 595, 85
- Crenshaw, D. M., Kraemer, S. B., & George, I. M. 2003, *ARA&A*, 41, 117
- Dadina, M., Cappi, M., Malaguti, G., Ponti, G., & de Rosa, A. 2005, *A&A*, 442, 461
- Dasgupta, S., Rao, A. R., Dewangan, G. C., & Agrawal, V. K. 2005, *ApJ*, 618, L87
- de la Calle & Loiseau N., 2009, User Guide to the XMM-Newton Science Analysis System, Issue 5.0, (http://xmm.esac.esa.int/external/xmm_user_support/documentation/sas_usg/USG/)
- Dickey, J. M., & Lockman, F. J. 1990, *ARA&A*, 28, 215
- Elvis, M. 2006, *Mem. Soc. Astron. Ital.*, 77, 573
- Freyberg, M. J., Briel, U. G., Dennerl, K., et al. 2004, *Proc. SPIE*, 5165, 112
- Kaspi, S., Maoz, D., Netzer, H., et al. 2005, *ApJ*, 629, 61
- Katayama, H., Takahashi, I., Ikebe, Y., Matsushita, K., & Freyberg, M. J. 2004, *A&A*, 414, 767
- King, A. R., & Pounds, K. A. 2003, *MNRAS*, 345, 657
- Krongold, Y., Nicastro, F., Elvis, M., et al. 2007, *ApJ*, 659, 1022
- Markowitz, A., Reeves, J. N., & Braitto, V. 2006, *ApJ*, 646, 783
- McKernan, B., Yaqoob, T., & Reynolds, C. S. 2004, *ApJ*, 617, 232
- McKernan, B., Yaqoob, T., & Reynolds, C. S. 2005, *MNRAS*, 361, 1337
- McKernan, B., Yaqoob, T., & Reynolds, C. S. 2007, *MNRAS*, 379, 1359
- Miniutti, G., & Fabian, A. C. 2006, *MNRAS*, 366, 115
- Miniutti, G., Ponti, G., Dadina, M., Cappi, M., & Malaguti, G. 2007, *MNRAS*, 375, 227
- Murray, N., Chiang, J., Grossman, S. A., & Voit, G. M. 1995, *ApJ*, 451, 498
- Nicastro, F., Fiore, F., Perola, G. C., & Elvis, M. 1999, *ApJ*, 512, 184
- Peterson, B. M., et al. 2004, *ApJ*, 613, 682
- Ponti, G., Ferrarese, L., Gilbert, K. M., et al. 2009, *MNRAS*, 236
- Porquet, D., Reeves, J. N., Uttley, P., & Turner, T. J. 2004, *A&A*, 427, 101
- Pounds, K. A., & Page, K. L. 2006, *MNRAS*, 372, 1275
- Pounds, K. A., & Reeves, J. N. 2008, [[arXiv:0811.3108](https://arxiv.org/abs/0811.3108)]
- Proga, D. 2003, *ApJ*, 592, L9
- Proga, D., & Kallman, T. R. 2004, *ApJ*, 616, 688
- Protassov, R., van Dyk, D. A., Connors, A., Kashyap, V. L., & Siemiginowska, A. 2002, *ApJ*, 571, 545
- Reeves, J. N., O’Brien, P. T., & Ward, M. J. 2003, *ApJ*, 593, L65
- Reeves, J., Done, C., Pounds, K., et al. 2008, *MNRAS*, 385, L108
- Risaliti, G., Bianchi, S., Matt, G., et al. 2005, *ApJ*, 630, L129
- Saez, C., Chartas, G., & Brandt, W. N. 2009, [[arXiv:0903.2878](https://arxiv.org/abs/0903.2878)]
- Schurch, N. J., & Done, C. 2007, *MNRAS*, 381, 1413
- Sim, S. A., Long, K. S., Miller, L., & Turner, T. J. 2008, *MNRAS*, 388, 611
- Smith, R. A. N., Page, M. J., & Branduardi-Raymont, G. 2007, *A&A*, 461, 135
- Tombesi, F., Cappi, M., Ponti, G., Malaguti, G., & Palumbo, G. G. C. 2008, *Mem. Soc. Astron. Ital.*, 79, 281
- Turner, T. J., Miller, L., Reeves, J. N., & Kraemer, S. B. 2007, *A&A*, 475, 121